Journal of Structural Geology 38 (2012) 243–253

Contents lists available at SciVerse ScienceDirect

Journal of Structural Geology

journal homepage: www.elsevier.com/locate/jsg

Effects of permeability and porosity evolution on simulated earthquakes

Andrea Bizzarri*

Istituto Nazionale di Geofisica e Vulcanologia, Sezione di Bologna, Via Donato Creti, 12, 40128 Bologna, Italy

ARTICLE INFO

Article history:
Received 24 January 2011
Received in revised form
20 June 2011
Accepted 23 July 2011
Available online 10 September 2011

Keywords:
Earthquake source dynamics
Rheology of faults
Frictional heating
Porosity
Earthquake recurrence
Computational seismology

ABSTRACT

Numerical simulations are a fundamental tool to access the typical conditions attained during earthquake instabilities and to simulate the large number of dissipative processes taking places during faulting. In this study we consider a single-degree-of-freedom spring-slider system, a simplified fault model which can describe the whole seismic cycle and the dynamics of a fault with spatially homogeneous properties. We assume a rate- and state-dependent friction in which we incorporate the effects of pore fluid pressure, thermally-pressurized as a consequence of the frictional heat produced during sliding. We explore, in a single framework, the role of the time variations of the porosity, permeability or both, ultimately leading to changes in hydraulic diffusivity, which has been recognized as one of the key parameters in thermally-pressurized faults. Our synthetic ruptures show that the changes in the hydraulic diffusivity only due to porosity variations do not markedly affect the earthquake recurrence (cycle time), the traction evolution and the thermal history of the fault. On the contrary, when the evolutions of both the porosity and the permeability are accounted for, the cycle time is significantly reduced. This result has a clear implication in the context of the hazard assessment.

1. Introduction

Recent laboratory experiments conducted at high slip velocities (about 1 m/s, thus comparable with cosesimic rates) and at moderate normal stresses (1–25 MPa, e.g., Sone and Shimamoto, 2009; Han et al., 2010; Di Toro et al., 2011) reveal a dramatic fault weakening, basically consisting in a severe reduction of the coefficient of friction (μ) with respect to the so-called Byerlee's value ($\mu \sim 0.6$; Byerlee, 1978). Several efforts have been spent in order to reproduce, at least qualitatively, this dramatic fault weakening by numerical models (i.e., in simulated earthquake ruptures), which has been proved to be more significant with respect to that predicted by classical, or canonical, formulations of governing models, such as the slip weakening law (Ida, 1972) and rate- and state-dependent friction laws (e.g., Ruina, 1983). As also pointed out by Noda et al. (2009) (see also Lachenbruch, 1980), the two physical phenomena most intensively studied are the thermally activated pore fluid pressurization and the flash heating of micro-asperity contacts. Experimental evidence of thermal pressurization (actually, thermochemical pressurization) has been reported by Ferri et al. (2010) and by De Paola et al. (2011). We also mention here that the contribution of thermal pressurization to the bulk weakening, at least in these experiments performed in non-cohesive rocks at very low normal stresses (<2 MPa), is limited to 10–20% of the total weakening (De Paola et al., 2011). The rest could be related to the so-called powder lubrication process (see Han et al., 2010; Reches and Lockner, 2010; Di Toro et al., 2011), which is not completely understood and which therefore cannot be incorporated in our modeling.

Both these two mechanisms, the thermal pressurization and the flash heating, have been adopted in the theoretical modeling of earthquake faulting (Bizzarri and Cocco, 2006a,b; Rice, 2006; Beeler et al., 2008; Bizzarri, 2009a; Noda et al., 2009 among others) and from these studies it emerged that the two keys parameters controlling the time evolution of the fault traction are *i*) the spatial extension of the slipping zone (where cosesimic slip localizes; Sibson, 2003), and *ii*) the hydraulic diffusivity ω (defined in next equation (4)).

Within the coseismic time scale (during which the stress is released and the seismic waves are excited by the earthquake source) the temporal evolution of the porosity tends to counterbalance the effect of the thermal pressurization and it is able to change the evolution of the traction within the cohesive zone (Bizzarri and Cocco, 2006b). Under some special assumptions (namely, when the slipping zone equals $2\sqrt{\omega T_{a.f.}}$—where ω is the hydraulic diffusivity defined in next equation (4) and $T_{a.f.}$ is the period of the spring-slider system—and when the parameter ε_{SR} in next equation (6) is large), these effects can eventually become even more relevant during the whole seismic cycle, as recently illustrated by Mitsui and Cocco (2010).

* Tel.: +39 051 4151432; fax: +39 051 4151499.
E-mail address: bizzarri@bo.ingv.it.

0191-8141/$ – see front matter © 2011 Elsevier Ltd. All rights reserved.
doi:10.1016/j.jsg.2011.07.009

In this paper we will consider the effects on the traction evolution of the time variations of the hydraulic diffusivity. In turn, the latter are caused by temporal changes of porosity and permeability, from which ω depends (see equation (4)). In particular, we will analyze the effects of the changes of ω with time on the evolution of the system in terms of the sliding velocity—which determines the recurrence time ($T_{\rm cycle}$), defined as the time interval separating two subsequent instabilities—, of the traction evolution and of the thermal history of the fault.

2. Solution of the elasto-dynamic equation

In the present study we will consider the spring-slider (or mass-spring) analog fault model, where a block of mass m (per unit surface) is subject to an external load (expressed by the temporally constant loading rate $\dot{\tau}_0 = k v_{\rm load}$) and slides on a planar slipping zone of thickness $2w$ against a frictional resistance τ. The second law of dynamics (i.e., the equation of motion) for such a system is that of a harmonic oscillator:

$$m\ddot{u} = k(u_{\rm load} - u) - \tau \tag{1}$$

in which the overdots indicate the time derivatives, k denotes the elastic constant of the spring (mimicking the elastic behavior of the medium surrounding the fault), $u_{\rm load}$ is the displacement of the loading point (which moves at the prescribed velocity $v_{\rm load} \equiv \dot{u}_{\rm load}$) and u is the displacement (which can be associate with the fault slip). The left-hand side term in equation (1) represents the inertia, which is accounted for only when the sliding velocity $v \equiv \dot{u}$ exceeds a critical value v_c; below v_c the quasi-static regime is considered, while above v_c we solve the complete system, as in Bizzarri (2010a). This implies a reduction of computational time and, moreover, the quasi-static regime solution agrees very well to the complete solution (where inertia is considered over the whole range of sliding velocity), as discussed in detail by Bizzarri and Belardinelli (2008). Fig. 1 schematically shows the fault model just described.

The traction τ specifies the constitutive law which governs the fault (see Bizzarri, 2009b, 2011c); here we assume the following rate- and state-dependent model (Linker and Dieterich, 1992):

$$\begin{cases} \tau = \left[\mu_* + a\ln\left(\dfrac{v}{v_*}\right) + b\ln\left(\dfrac{\Psi v_*}{L}\right)\right]\sigma_n^{\rm eff} \\ \dfrac{\mathrm{d}}{\mathrm{d}t}\Psi = 1 - \dfrac{\Psi v}{L} - \left(\dfrac{\alpha_{\rm LD}\Psi}{b\sigma_n^{\rm eff}}\right)\dfrac{\mathrm{d}}{\mathrm{d}t}\sigma_n^{\rm eff} \end{cases} \tag{2}$$

where a, b, L and $\alpha_{\rm LD}$ are the parameters accounting for the so-called direct effect of friction, its evolutionary weakening the relaxation of the state variable Ψ and the coupling between Ψ and the effective normal stress ($\sigma_n^{\rm eff} = \sigma_n - p_{\rm fluid}$, σ_n being the tectonic load and $p_{\rm fluid}$ being the pore fluid pressure), respectively. To better understand the effects of permeability and porosity evolutions on the system we assume here that all these constitutive parameters (a, b, L, $\alpha_{\rm LD}$ and σ_n) are constant through time; the role of temporal variations of a and b are discussed in Bizzarri (2011b). The evolution law for the state variable (also named ageing law) permits the friction to evolve on stationary contacts, in agreement with laboratory observations of Beeler et al. (1994).

In this work, accordingly to previous papers (Bizzarri and Belardinelli, 2008 and references cited therein) we define the

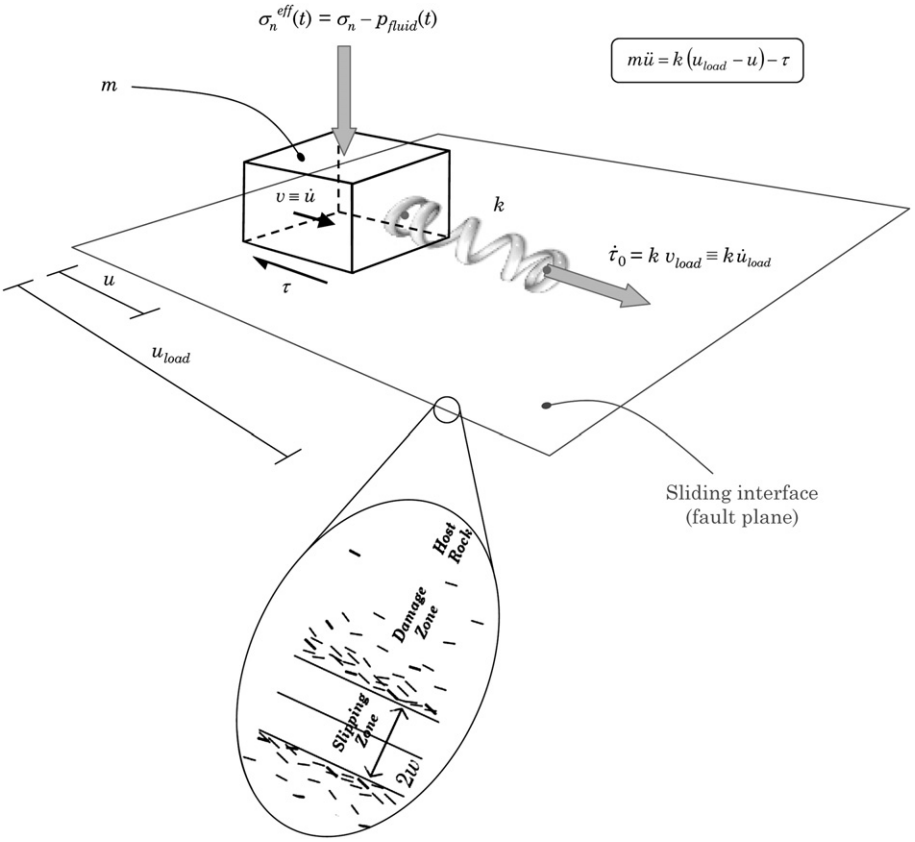

Fig. 1. Schematic representation of the fault analog model adopted in the present study. In agreement with geological observations (e.g., Sibson, 2003) a slipping zone of width $2w$ is surrounded by a damage zone. For simplicity we assume that $2w$ is temporally constant. From Bizzarri (2010a). Copyright 2010 American Geophysical Union. Reproduced by permission of American Geophysical Union.

time of an instability the instant when the sliding velocity exceeds a threshold value v_l (note that v_l is conceptually and numerically different with respect to the critical velocity v_c which, as discussed above, discriminates between quasi-static and dynamic regimes).

In a thermally-pressurized, fluid-saturated fault zone p_{fluid} evolves accordingly to the following relation (see Bizzarri and Cocco, 2006b for analytical details):

$$p_{\mathrm{fluid}}(t) = p_{\mathrm{fluid}_0} + \int_0^t \mathrm{d}t' \left\{ -\frac{\chi}{\omega-\chi}\,\mathrm{erf}\left(\frac{w}{2\sqrt{\chi(t-t')}}\right) + \frac{\omega}{\omega-\chi}\,\mathrm{erf}\left(\frac{w}{2\sqrt{\omega(t-t')}}\right)\right\}\left\{\frac{\gamma}{2w}\,\tau(t')v(t') - \frac{1}{\beta_{\mathrm{fluid}}\Phi(t')}\,\frac{\mathrm{d}}{\mathrm{d}t'}\,\Phi(t')\right\} \tag{3}$$

in which t is the time ($t \geq 0$), p_{fluid_0} is the initial pore fluid pressure, χ is the thermal diffusivity, erf(.) is the error function, γ is a dimensionless constant, w is the half-thickness of the slipping zone (Sibson, 2003; see also Fig. 1), β_{fluid} is the isothermal coefficient of compressibility of the fluid, Φ is the porosity and ω is the hydraulic diffusivity, which is defined as:

$$\omega = \frac{K}{\eta_{\mathrm{fluid}}\beta_{\mathrm{fluid}}\Phi} \tag{4}$$

where K is the permeability of the medium and η_{fluid} is the dynamic viscosity of the fluid (e.g., Andrews, 2002). The hydraulic diffusivity can change through time (thus exhibiting an implicit time dependence) due to temporal variations of porosity and permeability, as we will discuss is next sections 3 and 4, respectively.

The isothermal coefficient of compressibility of the fluid is defined as the inverse of the bulk modulus of elasticity of the fluid; namely: $\beta_{\mathrm{fluid}} = (1/\rho_{\mathrm{fluid}})(\partial\rho_{\mathrm{fluid}}/\partial p_{\mathrm{fluid}})|_{T=\mathrm{const}}$, where ρ_{fluid} is the cubic mass density of the fluid and partial derivatives are calculated for constant temperature (Batchelor, 1967). In general, β_{fluid} depends on the confining pressure and on the temperature (see Lachenbruch, 1980; his Fig. 1, and references cited therein and also Garagash and Rudnicki, 2003). This dependence is non linear and an analytical, quantitative interpretation of the reported data—which is necessary in order to include these variations in our model—is presently missed; therefore we have adopted an average value for the isothermal compressibility (see Table 2) representative of the whole range of temperatures and confining stresses realized in our numerical experiments.

Also the dynamic fluid viscosity can change due to temperature variations. If the fluid is pure water, an empirical description of this variation is expressed by the following relation: $\eta_{\mathrm{fluid}} = A10^{B/(T-C)}$, where the temperature T is in K, $A = 2.414 \times 10^{-5}$ Pa s, $B = 247.8$ K and $C = 140$ K (see Seeton, 2006 for a review). We will discuss this issue in Appendix A.

In the special case of temporally-constant porosity (i.e., for $\Phi(t) = \Phi(t=0) \equiv \Phi_0$, $\forall t \geq 0$) the last integrand term in equation (3) vanishes and therefore equation (3) simply reduces to the equation (9) of Bizzarri and Cocco (2006a). We also emphasize that for constant porosity the values of p_{fluid} are always positive, as Appendix B discusses. On the contrary, time variations of Φ can in principle counterbalance the effects of the heat source term $(\gamma/2w)\tau v$, ultimately leading to negative values of the integral in equation (3) and therefore causing a dilatant hardening effect (namely, negative pressure changes; $\Delta p_{\mathrm{fluid}} \equiv p_{\mathrm{fluid}} - p_{\mathrm{fluid}_0} < 0$).

Table 1
Reference parameters adopted in the present study. Initial conditions refer to $t = 0$.

Parameter	Value
Model parameters	
Tectonic loading rate, $\dot{\tau}_0 = k v_{\mathrm{load}}$	3.17×10^{-3} Pa/s (=1 bar/yr)
Machine stiffness, k	10 MPa/m[a]
Period of the analog freely slipping system, $T_{a.f.} = 2\pi\sqrt{m/k}$	5 s
Critical value of the sliding velocity above which the dynamic regime is considered, v_c	0.1 mm/s
Threshold value of the sliding velocity defining the occurrence of an instability, v_l	0.1 m/s[b]
Fault constitutive parameters	
Initial effective normal stress, $\sigma_{n_0}^{\mathrm{eff}} = \sigma_n - p_{\mathrm{fluid}_0}$	30 MPa
Logarithmic direct effect parameter, a	0.010
Evolution effect parameter, b	0.016
Characteristic scale length for the state variable evolution, L	1×10^{-2} m
Coupling between pore fluid pressure and state variable, α_{LD}	0.53
Reference value of the friction coefficient, μ_*	0.56
Reference value of the sliding velocity, v_*	3.17×10^{-10} m/s
Initial slip velocity, v_0	3.17×10^{-10} m/s
Initial value of state variable, Ψ_0	$\Psi^{ss}(v_0) = L/v_0 = 31.55 \times 10^6$ s[c]
Initial shear stress, τ_0	$\tau^{ss}(v_0) = \mu^* \sigma_{n0}^{\mathrm{eff}} = 16.8$ MPa[c]

[a] With the adopted constitutive parameters this corresponds to an unstable regime, in that $k < k_{\mathrm{cr}} \equiv (b-a)\sigma_n^{\mathrm{eff}}/L = 18$ MPa/m (Gu et al., 1984).
[b] In agreement with Bizzarri and Belardinelli (2008) and references cited therein.
[c] The system starts at $t = 0$ from its steady state (at a generic time t_* the steady state is defined by the condition $(\mathrm{d}/\mathrm{d}t)\Psi_{t=t_*}| = 0$).

In the numerical experiments presented and discussed in this paper the adopted parameters are listed in Tables 1 and 2, unless otherwise specified, while numerical details are summarized in Appendix C.

Table 2
Reference parameters pertaining to the thermal pressurization model and to the evolution laws for porosity and permeability. In the simulations with time variable porosity and permeability we use equations (6), (9) and (11) in order to start at $t = 0$ with values of K, Φ and ω identical to those pertaining to the reference case (K_0, Φ_0 and ω_0).

Parameter	Value
Thermal pressurization model (equation (3))	
Initial temperature, T_0	100 °C
Initial permeability, K_0	5×10^{-17} m^2
Initial hydraulic diffusivity, ω_0	0.02 m^2/s
Initial porosity, Φ_0	0.025
Heat capacity for unit volume of the bulk composite, c	3×10^6 J/(m^3 °C)
Thermal diffusivity, χ	1×10^{-6} m^2/s
Dimensionless parameter γ	0.5
Dynamic viscosity of the fluid, η_{fluid}	1×10^{-4} Pa s
Isothermal coefficient of compressibility of the fluid, β_{fluid}	1×10^{-9} Pa^{-1}
Slipping zone thickness, $2w$	2.2 mm
Porosity evolution law (equation (5))	
Reference value for the porosity, Φ_*	0.025
Coupling (sensitivity) parameter, $\varepsilon_{\mathrm{SR}}$	1.7×10^{-4}
Characteristic scale length for porosity evolution, L_{SR}	1×10^{-2} m (=L)
Permeability evolution – Rice's law (equation (8))	
Reference value for the permeability, K_*	1.35914×10^{-16} m^2
Reference value for the normal stress, σ_{n*}	30 MPa
Permeability evolution – Kozeny–Carman's law (equation (10))	
Dimensionless parameter K_{KC}	3.042×10^{-4}
(Average) diameter of grains, D_0	0.1 mm

3. Porosity evolution

The porosity of a porous material (rock or sediment) is the dimensionless ratio between the current fraction of voids (pore volume; V_{voids}) with respect to the total volume (V_{tot}) of the material: $\Phi = V_{voids}/V_{tot}$. By definition, Φ (sometime indicated with the symbol n) falls in [0,1]; $\Phi < 0.01$ for solid granite and $\Phi > 0.5$ for clay (e.g., Paterson and Wong, 2005). Fault zone porosity is expected to change during a cosesimic process due to the formation of the new cracks, changes to ineffective (or isolated) to effective (or connected) porosity (rearrangement of the interconnection chains between existing voids), grain size comminution, gouge evolution, etc. The time variations of Φ ultimately accounts for both frictional dilatancy ($\dot{\Phi} > 0$) and ductile compaction ($\dot{\Phi} < 0$). As comprehensively discussed by Bizzarri (2009b), in the literature several analytical expressions of the time evolution of the porosity have been introduced; in this study we adopt the widely used model proposed by Sleep (1995); see also Segall and Rice (1995), which is based on the critical state concept in soil mechanics, postulating the existence of a steady state porosity. In particular, Φ is assumed to be directly controlled by the evolution of the state variable Ψ:

$$\Phi = \Phi_* - \varepsilon_{SR} \ln\left(\frac{\Psi v_*}{L_{SR}}\right) \tag{5}$$

where Φ_* is a reference value for porosity and ε_{SR} is a sensitivity parameter (or dilatancy coefficient, roughly ranging between 5×10^{-5} and 3×10^{-4}; see Samuelson et al., 2009), which controls the amount of variation of Φ and which physically represents a measure of porosity changes caused by velocity variations (namely is: $\varepsilon_{SR} = \Delta\Phi/\Delta \ln(v)$). We assume here the same value of Φ_* adopted in previous studies (Andrews, 2002; Bizzarri and Cocco, 2006b; Mitsui and Cocco, 2010). L_{SR} is a characteristic scale length for the time evolution of Φ; laboratory experiments by Marone et al. (1990) indicate that in response to steps in slip velocity the porosity evolves toward a new steady state over a distance comparable to the evolution distance for the friction resistance (L). It is worth mentioning that the evolution law equation (5) refers to inelastic changes on pore volume (in other words the quantity Φ in equation (5) should be regarded as the plastic component of porosity). The inclusion of a thermoelastic part, due to changes of pore pressure and temperature with respect to the initial conditions, can eventually increase the effect of the plastic component of the porosity (Segall and Rice, 2006).

By considering the adopted initial conditions of the system (see Table 1), Φ_* is related to Φ_0 via the following relation:

$$\Phi_* = \Phi_0 + \varepsilon_{SR} \ln\left(\frac{L}{L_{SR}}\right) \tag{6}$$

We perform some numerical experiments by considering equation (5) and different values of the two relevant parameters, ε_{SR} (by keeping $L_{SR} = 1$ mm) and L_{SR} (by keeping $\varepsilon_{SR} = 1.1 \times 10^{-4}$). The results are reported in Figs. 2 and 3, respectively. A first outcome is that as the sensitivity parameter ε_{SR} increases we cannot observe a systematic trend in the peaks of slip velocity and in the recurrence time (Fig. 2a). Moreover, we can clearly see that, as expected, as ε_{SR} increases the variations of the porosity are larger (Fig. 2c). Correspondingly, the temporal changes of the hydraulic diffusivity are also larger, as predicted by its definition (see equation (4)). We recall here that we keep constant permeability and fluid viscosity in these simulations. However, the values attained by the effective normal stress (and thus by the fault traction) are not markedly different from those predicted by the reference model (black line in Fig. 2), in which we consider the thermal pressurization, but we keep the porosity (and thus ω) constant. At the same time, the temporal evolution of the fault temperature (Fig. 2b), which is expressed by

$$T(t) = T_0 + \frac{1}{2cw}\int_0^t dt' \ \mathrm{erf}\left(\frac{w}{2\sqrt{\chi(t-t')}}\right)\tau(t')v(t') \tag{7}$$

(Bizzarri and Cocco, 2006a; c is the heat capacity per unit volume of the bulk composite), confirms that the time evolution of the porosity is not able to significantly change the thermal history of the fault. We can also observe that in all cases the maximum temperature developed by frictional heat is roughly 1300 °C, which can cause the melting of rocks. However, the developed temperature does not exceed the effective melting temperature, above which the viscous rheology governs the fault (Bizzarri, 2011a). Although the presence of pseudotachylytes (solidified friction melts) decorating some exhumed faults suggests that friction melting occurs during some earthquakes, the abundance of pseudotachylyte remains debated (Sibson and Toy, 2006; Di Toro et al., 2006; Kirkpatrick et al., 2009). By reducing the size of the slipping zone thickness, the effective melting temperature can be exceeded, a continuous melt layer is then formed and the viscous rheology becomes paramount with respect to the Coulomb friction. Here we prefer to restrict our analysis to Coulombian rheology, in order to better focus on the effects of the variations of hydraulic diffusivity, permeability and porosity.

Compared to ε_{SR}, the changes in the length scale L_{SR} have relatively smaller effects on the fault system. In particular, the variations of the porosity (and thus those of the resulting hydraulic diffusivities) are smaller (compare Fig. 3c with Fig. 2c). At the same time, we cannot observe systematic trends in the recurrence time (Fig. 3a) and in the thermal history of the fault (Fig. 3b).

As an overall conclusion, we have seen that time variations of hydraulic diffusivity only due to porosity changes (we recall that Φ evolves accordingly to the model of Sleep (1995); equation (5)) do not markedly affect the earthquake recurrence (cycle time), the traction evolution and the thermal history of the fault.

4. Time evolution of the permeability

4.1. The Rice's model

The permeability physically represents a measure of the ability of a porous rock or an unconsolidated material to transmit fluids. It is often expressed through the hydraulic conductivity (κ) via $K = k(\eta_{fluid}/\rho_{fluid}g)$, where ρ_{fluid} is the cubic mass density of the fluid and g is the acceleration of gravity. In the special case of a single-phase porous material the permeability is an intensive property, i.e., it is a function of the material structure only and, as such, it is scale invariant (it does not depend on the amount of the porous material or on the system size). This is not the case in geological systems, where larger system sizes generally have larger conduits for fluid flow. Permeability enters as a part of the proportionality constant in the Darcy's law, expressing the volumetric flow rate of the fluid per unit area (q_ζ, also named Darcy's velocity) as a function of the pressure gradient (in one dimension we have: $q_\zeta = -(K/\eta_{fluid})(d/d_\zeta)p_{fluid}$). The estimation of the permeability is of pivotal importance in many areas of Earth sciences, thermal pressurization of pore fluids, magma degassing, hydrocarbon recovery, etc.

Unfortunately, though permeability measurements were performed in different rock types (e.g., Zhang et al., 1999; Faulkner and Rutter, 2001, 2003; Wibberley and Shimamoto, 2003), because of technical difficulties, this fundamental parameter is difficult to

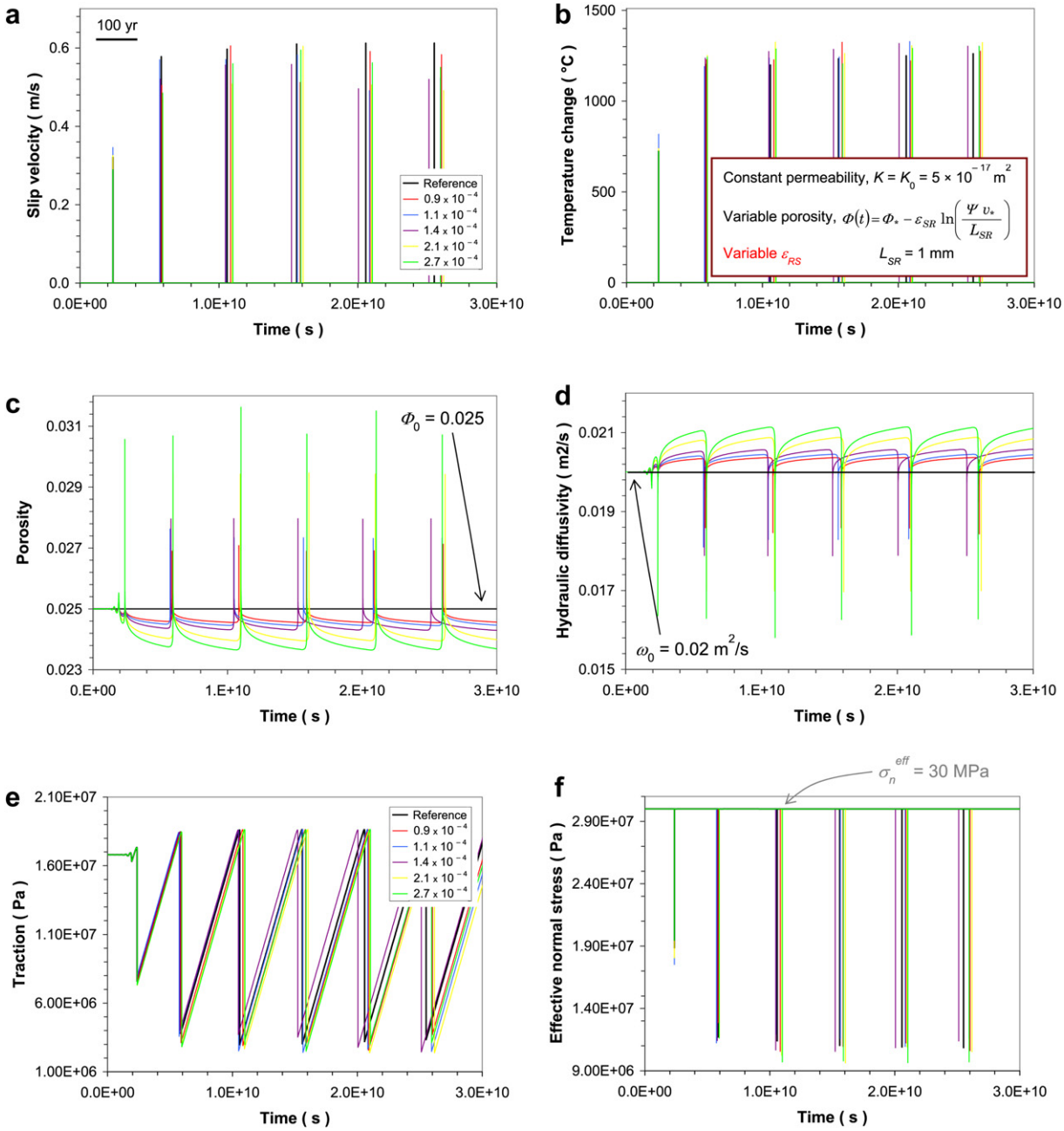

Fig. 2. Effects of the time evolution of the porosity Φ, which evolves accordingly to equation (5). In this case we have considered different values of the parameter ε_{SR} (values are indicated in the legend of panel (a)) with $L_{SR} = 1$ mm. Time histories of the slip velocity (panel (a)), of the temperature change with respect to the initial temperature T_0 (see equation (7); panel (b)), of the porosity (panel (c)), of the resulting hydraulic diffusivity (see equation (4); panel (d)), of the fault traction (panel (e)) and of the effective normal stress (panel (f)). Unless otherwise specified, in this and in the next figures all the parameters are those listed in Tables 1 and 2 and the reference case corresponds to a thermally-pressurized fault with constant porosity and permeability ($K(t) = K_0$ and $\Phi(t) = \Phi_0$, $\forall t \geq 0$).

estimate at seismic deformation conditions (i.e., for slip rate of 1 m/s). A first attempt was done by Tanikawa et al. (2012), but data are still very preliminary and cannot be incorporated in the models discussed here.

Local variations of the rock permeability have been inferred from observations of natural faults and from laboratory samples (Jourde et al., 2002; Brace et al., 1968; Huenges and Will, 1989). In this work we will consider two different evolution laws for permeability. The first, essentially due to Rice (1992), postulates an explicit dependence of K on the effective normal stress:

$$K(t) = K_* e^{-\frac{\sigma_n^{\mathrm{eff}}(t)}{\sigma_{n*}}} \tag{8}$$

in which K_* and σ_{n*} are reference values of permeability and normal stress, respectively. The second evolution law for the permeability is presented in section 4.2. The same relation was confirmed by Wibberley and Shimamoto (2005) for rocks sampled from the fault core of the Median Tectonic Line (Japan). For a given value of σ_{n*}, K_* is related to the initial permeability $K_0 \equiv K(t = 0)$ as follows:

$$K_* = K_0 e^{\frac{\sigma_{n_0}^{\mathrm{eff}}}{\sigma_{n*}}} \tag{9}$$

We explore the effects of the time variations of K according to equation (8) by changing the sensitivity parameter σ_{n*}; the results of the numerical experiments are reported in Fig. 4. Large increases

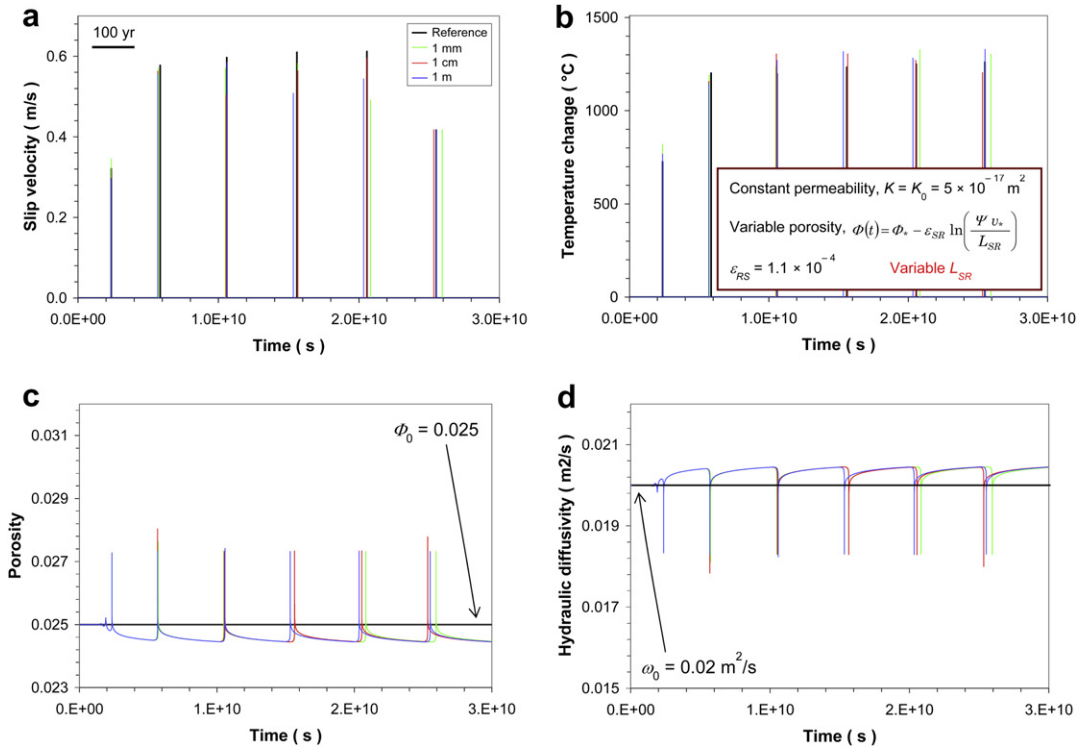

Fig. 3. The same as in Fig. 2, but now with different values of the length scale L_{SR}. (values are indicated in the legend of panel (a)). In this case $\varepsilon_{SR} = 1.1 \times 10^{-4}$.

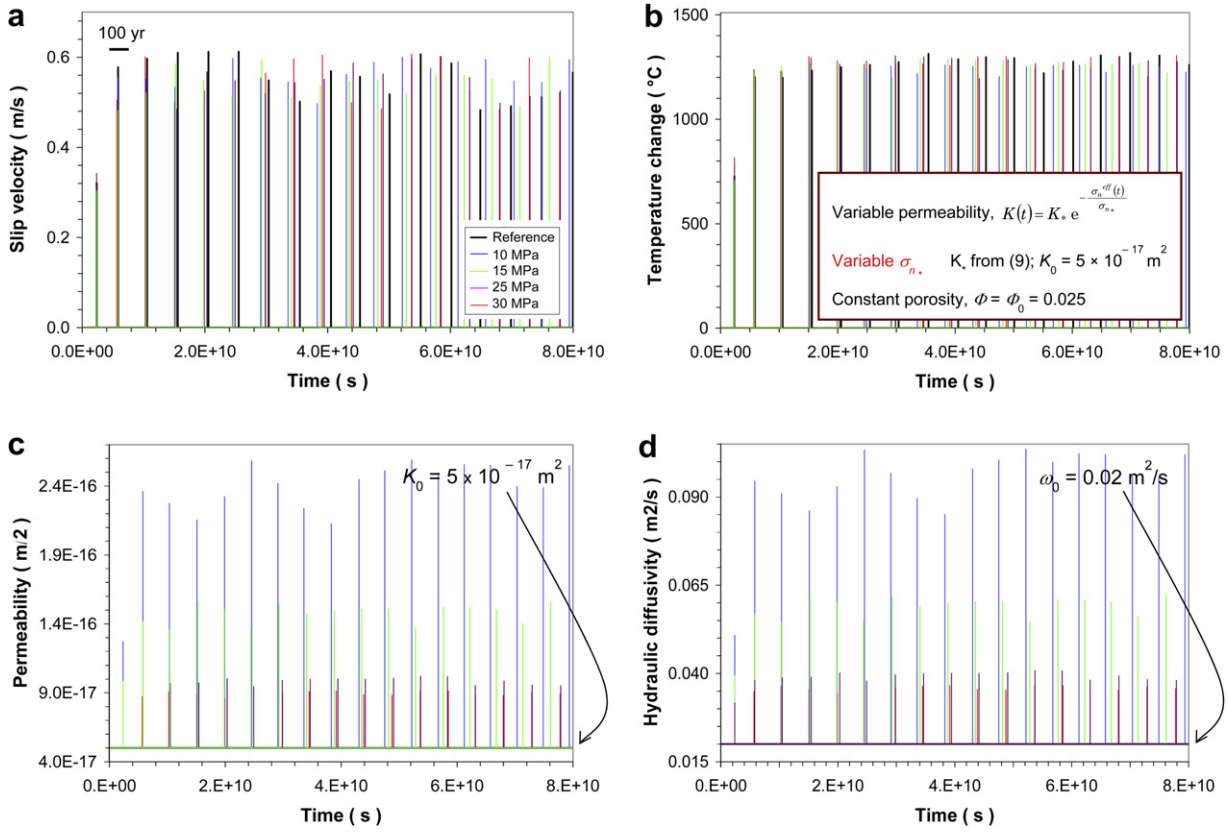

Fig. 4. Effects of the variation of the permeability K, which is assumed to evolve as described by equation (4). Time histories of the slip velocity (panel (a)), of the temperature change (panel (b)), of the permeability (panel (c)) and of the resulting hydraulic diffusivity (panel (d)). The porosity is constant in this case ($\Phi(t) = \Phi_0$, $\forall t \geq 0$).

in ω (reported in Fig. 4d) tend to anticipate an instability, thus reducing the seismic cycle, as it emerges from the location of the slip velocity peaks reported in Fig. 4a. As in the previous simulations, the thermal history of the fault is similar to the reference case (with constant hydraulic diffusivity) in that the peaks in T are roughly the same (Fig. 4b). We can see that as long as σ_{n^*} decreases the variations of K are more relevant (Fig. 4c); correspondingly, the changes in ω are also more relevant (Fig. 4d).

4.2. The Kozeny–Carman's model

The second evolution for K we consider consists in the Kozeny–Carman's model, which directly relates the permeability to the porosity (Kozeny, 1927; Carman, 1937). This amenable link between media properties and flow resistance inside pore channels suffers of the intrinsic difficulty of evaluating in detail the spatial shape of the channels and their distribution. Among the large number of the formulations of the Kozeny–Carman's relation (see also Costa, 2006 for a discussion) we adopt here the following equation:

$$K(t) = K_{KC}\frac{(\Phi(t))^3}{(1-\Phi(t))^2}(D(t))^2 \tag{10}$$

being K_{KC} a dimensionless parameter (which generally depends on the material; see Costa, 2006 and references cited therein) and D the (average) diameter of grains (ranging between 4×10^{-5} m and 1×10^{-4} m; see Niemeijer et al., 2010). The explicit time dependence of D in equation (10) accounts for possible gouge refinement and fragmentation; in the present approach, however, we will simply consider a constant diameter $D = D_0$ (therefore equation (10) is equivalent to the relation $K(t) = K'_{KC}((\Phi(t))^3/(1-\Phi(t))^2)$, with $K'_{KC} \equiv K_{KC}D_0^2$). We do not want overemphasize that in this case only a time variable porosity causes temporal changes in K. Finally, we note that, for a given diameter, at $t = 0$ it holds:

$$K_{KC} = \frac{K_0}{D_0^2}\frac{(1-\Phi_0)^2}{\Phi_0^3} \tag{11}$$

We report in Fig. 5 the results obtained by comparing a reference case, with both porosity and permeability temporally constant (black lines), a situation when only Φ is evolving according to equation (5) (red lines) and a case in which both Φ and K evolve (in the latter configuration K follows equation (11); blue lines). While in the case of constant permeability the time evolution of the porosity does not alter the whole behavior of the fault (as already observed in section 3), by considering both the variations of Φ and K we can see that the cycle time is reduced (Fig. 5a). As a result, the time variations of the pore fluid pressure in the correspondence of the dynamic events are smaller in the case of the Kozeny–Carman's model with respect to the other simulations (Fig. 5b). This ultimately leads to a reduction of the frictional resistance (we recall here that $\tau = \mu(\sigma_n - p_{\text{fluid}})$) and this causes an anticipation of the occurrence of earthquakes (Fig. 5a). Indeed, by looking at Fig. 5d, we see that the time evolution of the porosity causes a small increase of the hydraulic diffusivity during the interseismic period and a more relevant decrease in the correspondence of the

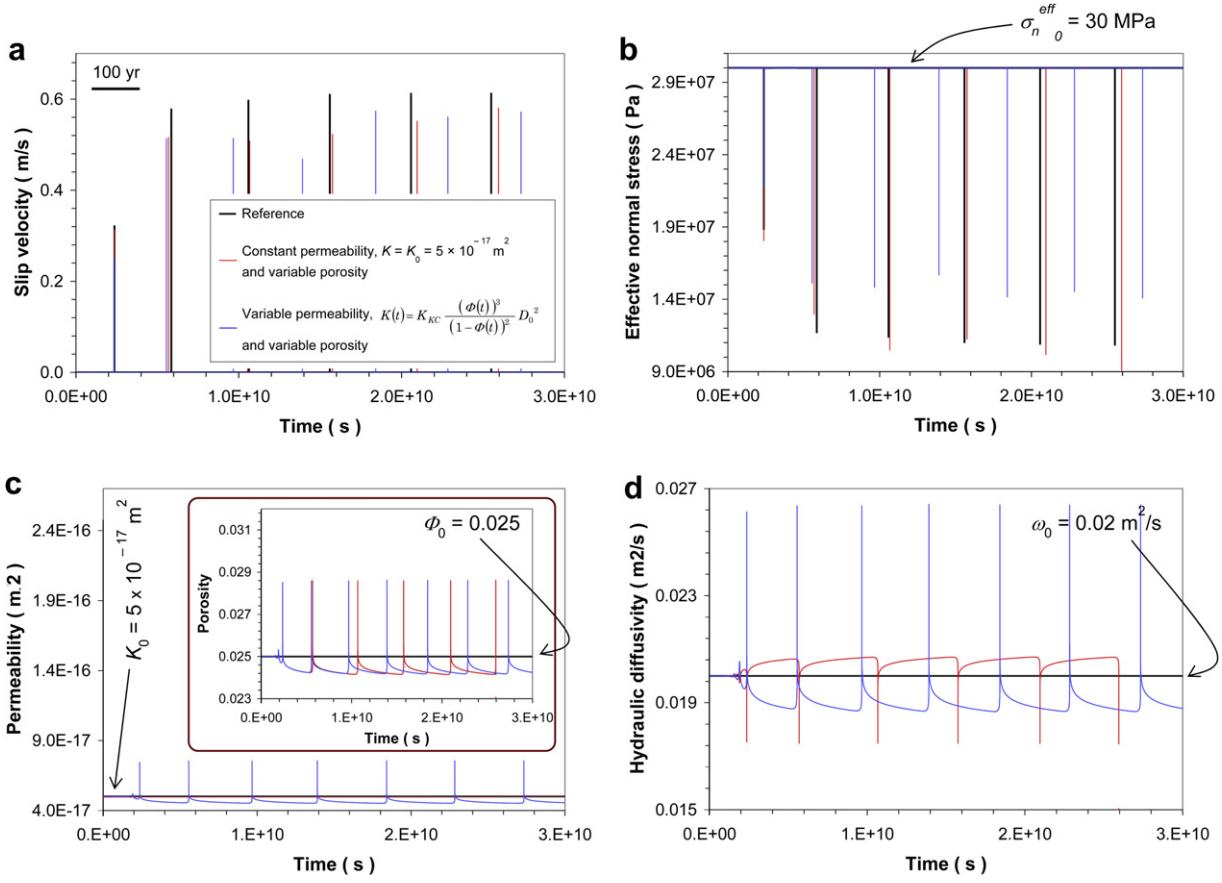

Fig. 5. Effects of the variations of the permeability, which now follows equation (10); in this case also the porosity changes through time, as in equation (5). Time histories of the slip velocity (panel (a)), of the effective normal stress $\sigma_n^{\text{eff}} = \sigma_n - p_{\text{fluid}}$, with p_{fluid} as in equation (3) (panel (b)), of the permeability, with inset reporting that of the porosity (panel (c)), and of the resulting hydraulic diffusivity (panel (d)).

instability events (see also previous Figs. 2d and 3d). Conversely, the evolution of K tends to do the opposite (see also Fig. 4d). The inclusion of the Kozeny–Carman's model shows that the evolution of K dominates that of Φ.

5. Discussion and conclusions

In this paper we have considered the spring-slider dashpot model to numerically model the whole cycle of a fluid-saturated seismogenic fault, obeying a rate- and state-dependent friction. In particular, we assumed that the fault is described by the Linker–Dieterich's constitutive model (equation (2)), in which the pore fluid pressure evolution is given by the analytical solution of Bizzarri and Cocco (2006a,b; equation (3)).

Rock–fluid interaction is an important phenomenon connected with tectonic instability, in that faulting processes affect the fluid pressure and the fluid pressure concurs to approach faulting conditions (e.g., Engelder and Lacazette, 1990; Merlani and Natale, 2001; Jonsson et al., 2003). In the thermal pressurization model the two most important parameters controlling the time evolution of the fault traction are the size of the slipping zone where the deformation is concentrated ($2w$; see Fig. 1) and the hydraulic diffusivity (ω; see equation (4)). It has been shown that the temporal variations of w due to wear processes can significantly modify the duration of the seismic cycle (inter-event time), complicating the predictability of a subsequent instability event, even in the simplest (and idealized) configuration of a single and isolated fault (Bizzarri, 2010a).

The main focus of the present paper is on the time variations of the hydraulic diffusivity. Actually, ω can change as a consequence of permeability and porosity changes or both (see sections 3 and 4). Large variations of ω are concentrated within the time window of the dynamic instability, during which large changes of effective normal stress and state variable (and therefore those of permeability and porosity) occur.

Permeability and porosity evolve during the seismic cycle also for chemical effects (e.g., fault healing and sealing due to mineral precipitation). The effectiveness of these healing processes is evident in field studies of exhumed seismogenic faults but also recognized in the evolution of the v_P/v_S ratio in the fault zone with time after moderate to large earthquakes. These permeability changes can have relevant effects in the rheology of the fault, in earthquake recurrence time (they control the elastic stiffness and the capacity of the wall rocks to store the elastic strain energy), in the potential activation of the weakening mechanism during coseismic slip, and in the seismic cycle in general (Rutter, 1976; Gratier et al., 2003, 2009; Gratier, in press). In the present study we neglect these chemical effects in that we do not presently have a mathematical model to properly interpret the information mentioned above.

Due to the point-like nature of the presently adopted fault analog model we disregard any complication arising from the spatial heterogeneities of ω that have been considered in a different study (Noda and Lapusta, 2010). This model is very idealized, but nevertheless it can be useful to gain some understanding of the role of different physical effects.

Our numerical experiments show that the time variations of the hydraulic diffusivity only caused by the evolution of the porosity (we have assumed in this paper that Φ evolves accordingly to the model of Sleep (1995); see equation (5)) do not significantly affect the earthquake recurrence (cycle time), the traction evolution and the thermal history of the fault (Figs. 2 and 3). This result agrees with previous findings of Mitsui and Cocco (2010).

Moreover, the time variations of the permeability alone, in agreement to the Rice (1992)'s model (equation (9)) cause large increases in ω that tend to anticipate an instability and therefore tend to reduce the seismic cycle (Fig. 4). As in the previous case, the thermal history of the fault is similar to the reference case (with constant hydraulic diffusivity) in that the peaks in T are roughly the same.

On the contrary, we have shown that the incorporation of variations of both porosity and permeability (thought the implementation of the Kozeny–Carman's model; equation (10)) produces a significant reduction in the seismic cycle (Fig. 5). This result might have relevant implications in the context of hazard assessment and damage mitigations scenarios.

As a further development of this work it would be interesting to test different evolution equations for the porosity (see Bizzarri, 2009b and references cited therein for a review) as more observation constraints will be available. Additionally, other weakening mechanisms, different from the thermal pressurization of pore fluid considered here—the powder lubrication (Han et al., 2010, 2011; De Paola et al., 2011; Reches and Lockner, 2010; Di Toro et al., 2011), the elastohydrodynamic lubrication (Brodsky and Kanamori, 2001) and chemical mechanisms (Sulem and Famin, 2009; Brantut et al., 2010)—, will be considered in future works.

Acknowledgments

Part of this work originated from the insightful discussions I had the pleasure to have during the workshop "Physico-chemical processes in seismic faults" held in Padova, November 2010, founded by Progetti di Eccellenza, Fondazione Cassa di Risparmio di Padova e Rovigo (CARIPARO). L. Fucci is kindly acknowledged for assisting in the preparation of some figures. Finally, I thank the Associate Editor, G. Di Toro, and two anonymous referees for their useful comments.

Appendix A. Effects of the temperature on the dynamic fluid viscosity

As mentioned in section 2, the dynamic viscosity of the fluids η_{fluid} can change with the ambient temperature. For water an empirical relation describing such a variation reads:

$$\eta_{\mathrm{fluid}} = A\, 10^{\frac{B}{T-C}} \tag{A.1}$$

where the temperature T is now expressed in K and the empirical constants are: $A = 2.414 \times 10^{-5}$ Pa s, $B = 247.8$ K and $C = 140$ K (see Seeton, 2006 for a review). The behavior of the dynamic viscosity as predicted by equation (A.1) is reported in Fig. A.1a, for the typical temperatures realized in our numerical experiments.

The resulting hydraulic diffusivity changes, as expected from equation (4), as the temperature due to sliding evolves; this is visible from Fig. A.1d. The variations of ω are smaller than those observed in the configurations where permeability or porosity vary (see Figs. 2d, 3d and 4d and 5d). Accordingly, the time evolution of the sliding velocity is very similar in the two cases (Fig. A.1b) because the variations of the effective normal stress are also small (Fig. A.1c). We can note that, due to the different value of the dynamic fluid viscosity at $t = 0$, the system has a different evolution at the beginning of the life of the fault. When the system enters in its limiting cycle, then the inter-event time is the constant in both the cases.

Appendix B. Positiveness of the pore fluid pressure in the absence of porosity changes

Let we consider the pore fluid pressure evolution in the special case of temporally-constant porosity. Under this hypothesis equation (3) becomes:

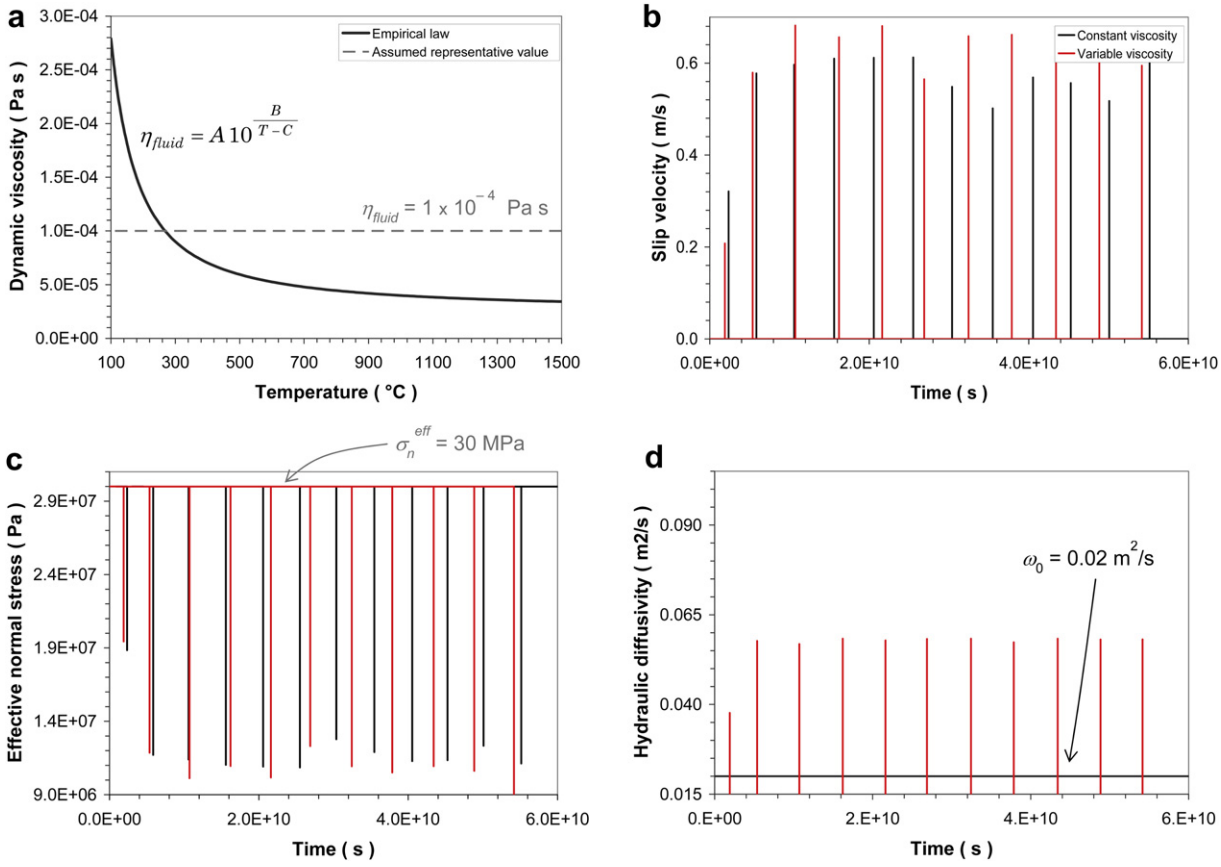

Fig. A.1. (a) Evolution of the dynamic viscosity of the water as a function of the temperature T in the range covered by the simulations presented in the paper. The black line represents the empirical relation (A.1). For comparison, the assumed value of η_{fluid} is superimposed as dashed gray line. Panels (b) to (d) reports the comparison between the reference configuration, with constant viscosity (black lines), and the case where η_{fluid} varies with T accordingly to equation (A.1) (red curves). (b) Evolution of the sliding velicity. (c) Effective normal stress. (d) Resulting hydraulic diffusivity.

$$p_{\text{fluid}}(t) = p_{\text{fluid}_0} + \frac{\gamma}{2w}\int_0^t \mathrm{d}t' \frac{\omega \operatorname{erf}\left(\frac{C}{\sqrt{\omega}}\right) - \chi \operatorname{erf}\left(\frac{C}{\sqrt{\chi}}\right)}{\omega - \chi}\tau(t')v(t') \tag{B.1}$$

where $C \equiv w/(2\sqrt{t-t'})$. For all times t' the integrand function is positive, because τ and v are positive by definition and $\omega > \chi$. Moreover, it holds:

$$\frac{\operatorname{erf}\left(\frac{C}{\sqrt{\chi}}\right)}{\operatorname{erf}\left(\frac{C}{\sqrt{\omega}}\right)} < \frac{\omega}{\chi} \tag{B.2}$$

In fact, by considering the Taylor expansion of the error function at the first order, we can rewrite equation (B.2) as follows:

$$\frac{\frac{C}{\sqrt{\chi}}}{\frac{C}{\sqrt{\omega}}} < \frac{\omega}{\chi} \tag{B.3}$$

Equation (B.3) is obviously satisfied because $\omega/\chi > 1$. We emphasize that the positiveness of p_{fluid} holds also in cases when hydraulic diffusivity changes through time.

Appendix C. Numerical solution of the elasto-dynamic problem

The elasto-dynamic problem for our 1-D fault system is solved numerically by using the fourth-order Runge–Kutta algorithm with auto-adaptive time stepping (Press et al., 1992). Our numerical code, which implements the algorithms `RKQC` and `RK4` of Press et al. (1992) gives the same results as the `ODE45` routine in Matlab® (see Matlab® documentation), used by other authors (e.g., Kato, 2001; de Loremzo and Loddo, 2010). Namely, we numerically integrate the equation of motion (1), coupled with the constitutive equations (2) and (3).

We simply recall here that the analytical solution (3) expresses the temporal evolution of the pore fluid pressure as a function of the slip velocity and traction history. This equation been derived in Bizzarri and Cocco (2006b), by considering the mass conservation, spatially homogeneous properties of fault zone (namely the dimensionless parameter γ in equation (3), the fluid compressibility, the porosity and its time derivative do not depend on the spatial coordinates). In the thermal pressurization model of Bizzarri and Cocco (2006a,b) the fluids migrates in a direction perpendicular to the fault. Equation (3) also assumes that advective terms are neglected, but the error is expected to be small, as discussed by Andrews (2002).

The scale length of equation (3) is the thermal boundary layer, which is expressed as $\delta_t = \sqrt{2\chi t_d}$, where χ is thermal diffusivity of rocks and t_d is the duration of slip (e.g., Fialko, 2004); typically, $\delta \sim$ few centimeter. More recently, Mitsui and Cocco (2010)

introduced another scale length to characterize the thermal pressurization process, which is the hydraulically activated layer $\delta_h = 2\sqrt{\omega\, T_{a.f.}}$, where ω is the hydraulic diffusivity and $T_{a.f.}$ is the period of the analog freely slipping system (see Table 1). For our reference parameters, $\delta_h = 0.63$ m.

The quantity $\tau v/2w$ appearing in equation (3)—and in the evolution of the temperature developed by frictional heat as well (equation (7))—represents the time variable heat input, under the assumption that all work spent during sliding is dissipated through frictional heating. This is quite reasonable, as discussed in more detail in Pittarello et al. (2008).

Formally, to obtain the analytical solutions (3) and (7), we solve the 1-D Fourier's heat conduction equations with a heat source function which equals $\tau v/2w$ within the slipping zone thickness $2w$ where the deformation is concentrated and vanishes outside $2w$. In the literature (e.g., Andrews, 2002; Noda et al., 2009) it has been also considered a Gaussian-shaped heat source function, in which the heat decreases as a Gaussian function as the distance from the center of the slipping zone increases. A synoptic comparison between these two heat source models (Bizzarri, 2010c) revealed that the resulting time histories of the temperature variations due to fault slip converge to the same result for small values of $2w$ (namely, for $w < 0.01$ mm for typical parameters), while the Gaussian-shaped function tends to predict lower temperatures than those obtained by adopting the source function used in the present study. Both the above mentioned heat sources are more realistic generalization of the frictional heating model which assumes that all the developed heat is concentrated on a mathematical plane having null thickness (e.g., McKenzie and Brune, 1972; Richards, 1976; Kato, 2001). The latter predicts overestimates of the developed temperatures, as shown by Bizzarri (2010b).

The hydraulic diffusivity ω appearing in equation (3) is defined in equation (4). Depending on the configurations we consider, such an equation is then coupled with equations (5), (8) and (10), which account for possible time variations of porosity and permeability.

As mentioned in section 2 for sliding velocity lower than the critical value of $v_c = 0.1$ mm/s the quasi-static equation is solved; in this case the left hand side member of equation (1) is taken as zero, in that inertial effects are neglected in the pre-seismic and inter-seismic phases.

References

Andrews, D.J., 2002. A fault constitutive relation accounting for thermal pressurization of pore fluid. J. Geophys. Res. 107 (B12), 2363. doi:10.1029/2002JB001942.

Batchelor, G.H., 1967. An Introduction to Fluid Dynamics. Cambridge Univ. Press, New York, 615 pp.

Beeler, N.M., Tullis, T.E., Goldsby, D.L., 2008. Constitutive relationships and physical basis of fault strength due to flash heating. J. Geophys. Res. 113, B01401. doi:10.1029/2007JB004988.

Beeler, N.M., Tullis, T.E., Weeks, J.D., 1994. The roles of time and displacement in the evolution effect in rock friction. Geophys. Res. Lett. 21 (18), 1987–1990. doi:10.1029/94GL01599.

Bizzarri, A., 2009a. Can flash heating of asperity contacts prevent melting? Geophys. Res. Lett. 36, L11304. doi:10.1029/2009GL037335.

Bizzarri, A., 2009b. What does control earthquake ruptures and dynamic faulting? A review of different competing mechanisms. Pure Appl. Geophys. 166 (5–7), 741–776. doi:10.1007/s00024–009–0494–1.

Bizzarri, A., 2010a. On the recurrence of earthquakes: role of wear in brittle faulting. Geophys. Res. Lett. 37, L20315. doi:10.1029/2010GL045480.

Bizzarri, A., 2010b. Determination of the Temperature Field Due to Frictional Heating on a Sliding Interface. I.N.G.V. Technical Reports 158, pp. 1–16. Available from: http://portale.ingv.it/portale_ingv/produzione-scientifica/rapporti-tecnici-ingv/archivio/copy_of_numeri-pubblicati-2010/.

Bizzarri, A., 2010c. Comparison between Different Heat Source Functions in Thermal Conduction Problems. I.N.G.V. Technical Reports 171, pp. 1–18. Available from: http://portale.ingv.it/portale_ingv/produzione-scientifica/rapporti-tecnici-ingv/archivio/copy_of_numeri-pubblicati-2010/.

Bizzarri, A., 2011a. Dynamic seismic ruptures on melting fault zones. J. Geophys. Res. 116, B02310. doi:10.1029/2010JB007724.

Bizzarri, A., 2011b. Temperature variations of constitutive parameters can significantly affect the fault dynamics. Earth Plan. Sci. Lett. 306, 272–278. doi:10.1016/j.epsl.2011.04.009.

Bizzarri, A., (2011)c. On the deterministic description of earthquakes. Rev. Geophys., 49, RG3002. doi:10.1029/2011RG000356.

Bizzarri, A., Belardinelli, M.E., 2008. Modelling instantaneous dynamic triggering in a 3-D fault system: application to the 2000 june South Iceland seismic sequence. Geophys. J. Int. 173, 906–921. doi:10.1111/j.1365–246X.2008.03765.x.

Bizzarri, A., Cocco, M., 2006a. A thermal pressurization model for the spontaneous dynamic rupture propagation on a three-dimensional fault: 1. Methodological approach. J. Geophys. Res. 111, B05303. doi:10.1029/2005JB003862.

Bizzarri, A., Cocco, M., 2006b. A thermal pressurization model for the spontaneous dynamic rupture propagation on a three-dimensional fault: 2. Traction evolution and dynamic parameters. J. Geophys. Res. 111, B05304. doi:10.1029/2005JB003864.

Brace, W.F., Walsh, J.B., Frangos, W.T., 1968. Permeability of granite under high pressure. J. Geophys. Res. 73 (6), 2225–2236.

Brantut, N., Schubnel, A., Corvisier, J., Sarout, J., 2010. Thermochemical pressurization of faults during cosesimic slip. J. Geophys. Res. 115, B05314. doi:10.1029/2009JB006533.

Brodsky, E.E., Kanamori, H., 2001. Elastohydrodynamic lubrication of faults. J. Geophys. Res. 106 (B8), 16,357–16,374.

Byerlee, J.D., 1978. Friction of rocks. Pure Appl. Geophys. 116, 615–626. doi:10.1007/BF00876528.

Carman, P., 1937. Fluid flow through a granular bed. Trans. Inst. Chem. Eng. 15, 150–167.

Costa, A., 2006. Permeability-porosity relationship: a reexamination of the Kozeny–Carman equation based on a fractal pore-space geometry assumption. Geophys. Res. Lett. 33, L02318. doi:10.1029/2005GL025134.

de Loremzo, S., Loddo, M., 2010. Effect of frictional heating and thermal advection on pre-seismic sliding: a numerical simulation using a rate-, state- and temperature-dependent friction law. J. Geodyn. 49, 1–13. doi:10.1016/j.jog.2009.07.001.

De Paola, N., Hirose, T., Mitchell, T., Di Toro, G., Togo, T., Shimamoto, T., 2011. Fault lubrication and earthquake propagation in thermally unstable rocks. Geology 39, 35–38.

Di Toro, G., Han, R., Hirose, T., De Paola, N., Nielsen, S., Mizoguchi, K., Ferri, F., Cocco, M., Shimamoto, T., 2011. Fault lubrication during earthquakes. Nature 471, 494–498.

Di Toro, G., Hirose, T., Nielsen, S., Shimamoto, T., 2006. Relating high-velocity rock friction experiments to coseismic slip. In: Abercrombie, R., McGarr, A., Di Toro, G., Kanamori, H. (Eds.), Radiated Energy and the Physics of Faulting. Geophysical Monograph Series, vol. 170. American Geophysical Union, Washington, D.C, pp. 121–134.

Engelder, T., Lacazette, A., 1990. Natural hydraulic fracturing. In: International Symposium on Rock Joints, Loen, pp. 35–43.

Faulkner, D.R., Rutter, E.H., 2001. Can the maintenance of overpressured fluids in large strike-slip fault zones explain their apparent weakness? Geology 29 (6), 503–506.

Faulkner, D.R., Rutter, E.H., 2003. The effect of temperature, the nature of the pore fluid, and subyield differential stress on the permeability of phyllosilicate-rich fault gouge. J. Geophys. Res. 108 (B5), 2227,. doi:10.1029/2001JB001581.

Ferri, F., Di Toro, G., Hirose, T., Shimamoto, T., 2010. Evidences of thermal pressurization in high velocity friction experiments on smectite-rich gouges. Terra Nova 22, 347–353.

Fialko, Y., 2004. Temperature fields generated by the elastodynamic propagation of shear cracks in the earth. J. Geophys. Res. 109, B01303. doi:10.1029/2003JB002497.

Garagash, D.I., Rudnicki, J.W., 2003. Shear heating of a fluid-saturated slip-weakening dilatant fault zone, 1, limiting regimes. J. Geophys. Res. 108 (B2), 2121. doi:10.1029/2001JB001653.

Gratier, J.–P. Fault permeability and strength evolution related to fracturing and healing episodic processes (years to millennia) the role of pressure solution, Oil Gas Sci. Technol. 66 (2), in press.

Gratier, J.–P., Favreau, P., Renard, F., 2003. Modeling fluid transfer along Californian faults when integrating pressure solution crack sealing and compaction process. J. Geophys. Res. 108 (B2), 28–52.

Gratier, J.–P., Guiguet, R., Renard, F., Jenatton, L., Bernard, D., 2009. A pressure solution creep law for quartz from indentation experiments. J. Geophys. Res. 114, B03403. doi:10.1029/2008JB005652.

Gu, J.C., Rice, J., Ruina, A.L., Tse, S.T., 1984. Slip motion and stability of a single degree of freedom elastic system with rate and state dependent friction. J. Mech. Phys. Solids 32, 167–196.

Han, R., Hirose, H., Shimamoto, T., 2010. Strong velocity weakening and powder lubrication of simulated carbonate faults at seismic slip rates. J. Geophys. Res. 115, B03412. doi:10.1029/2008JB006136.

Han, R., Hirose, T., Shimamoto, T., Lee, Y., Ando, J.i, 2011. Granular nanoparticles lubricate faults during seismic slip. Geology 39, 599–602.

Huenges, E., Will, G., 1989. Permeability, bulk modulus and complex resistivity in crystalline rocks. In: Bridgwater, D. (Ed.), Fluids Movements – Element Transport and the Composition of the Deep Crust. Kluwed, Dordrecht, pp. 361–375.

Ida, Y., 1972. Cohesive force across the tip of a longitudinal–shear crack and Griffith's specific surface energy. J. Geophys. Res. 77 (20), 3796–3805.

Jonsson, S., Segall, P., Pedersen, R., Bjornsson, G., 2003. Post-earthquake ground movements correlated to pore pressure transients. Nature 424, 179–183.

Jourde, H., Flodin, E.A., Aydin, A., Durlofsky, L.J., Wen, X.H., 2002. Computing permeability of fault zones in eolian sandstone from outcrop measurements. AAPG Bull. 86, 1187–1200.
Kato, N., 2001. Effect of frictional heating on pre-seismic sliding: a numerical simulation using a rate-, state- and temperature-dependent friction law. Geophys. J. Int. 147, 183–188.
Kirkpatrick, J.D., Shipton, Z.K., Persano, C., 2009. Pseudotachylytes: rarely generated, rarely preserved, or rarely reported? Bull. Seismol. Soc. Am. 99 (1). doi:10.1785/0120080114.
Kozeny, J., 1927. Uber kapillare leitung der wasser in boden. Sitzungsber. Akad. Wiss. Wien 136, 271–306 (in German).
Lachenbruch, A.H., 1980. Frictional heating, fluid pressure, and the resistance to fault motion. J. Geophys. Res. 85, 6097–6122.
Linker, M.F., Dieterich, J.D., 1992. Effects of variable normal stress on rock friction: observations and constitutive equations. J. Geophys. Res. 97, 4923–4940.
Marone, C., Raleigh, B.B., Scholx, C.H., 1990. Frictional behavior and constitutive modeling of simulated gouge. J. Geophys. Res. 95 (B5), 7007–7025. doi:10.1029/095iB05p07007.
McKenzie, D., Brune, J.N., 1972. Melting on fault planes during large earthquakes. Geophys. J. Roy. Astron. Soc. 29, 65–78.
Merlani, A., Natale, G., 2001. Fracturing processes due to temperature and pressure nonlinear waves propagating in fluid-saturated porous rock. J. Geophys. Res. 106 (B6), 11067–11081.
Mitsui, Y., Cocco, M., 2010. The role of porosity evolution and fluid flow in frictional instabilities: a parametric study using a spring-slider dynamic system. Geophys. Res. Lett. 37, L233305. doi:10.1029/2010GL045672.
Niemeijer, A., Marone, C., Elsworth, D., 2010. Frictional strength and strain weakening in simulated fault gouge: competition between geometrical weakening and chemical strengthening. J. Geophys. Res. 115, B10207. doi:10.1029/2009JB000838.
Noda, H., Dunham, E.M., Rice, J.R., 2009. Earthquake ruptures with thermal weakening and the operation of major faults at low overall stress levels. J. Geophys. Res. 114, B07302. doi:10.1029/2008JB006143.
Noda, H., Lapusta, N., 2010. 3D earthquake sequence simulations with evolving temperature and pore pressure due to shear heating: effect of heterogeneous hydraulic diffusivity. J. Geophys. Res. 115, B12314. doi:10.1029/2010JB007780.
Paterson, M.S., Wong, T.–F., 2005. Experimental Rock Deformation. Springer.
Pittarello, L., Di Toro, G., Bizzarri, A., Pennacchioni, G., Hadizadeh, J., Cocco, M., 2008. Energy partitioning during seismic slip in pseudotachylytes-bearing faults (Gole Larghe fault, Adamello, Italy). Earth Plan. Sci. Lett. 269, 131–139. doi:10.1016/j.epsl.2008.01.052.
Press, W.H., Teukolsky, B.P., Vetterling, W.T., 1992. Numerical Recipes, second ed. Cambridge University Press, New York.
Reches, Z., Lockner, D.A., 2010. Fault weakening and earthquake instability by powder lubrication. Nature 467, 452–455.
Rice, J.R., 1992. Fault stress states, pore pressure distributions, and the weakness of the San Andreas Fault. In: Evans, B., Wong, T.–F. (Eds.), Fault Mechanics and Transport Properties in Rocks. Academic, San Diego, CA, USA, pp. 475–503.
Rice, J.R., 2006. Heating and weakening of faults during earthquake slip. J. Geophys. Res. 111 (B5), B05311. doi:10.1029/2005JB004006.
Richards, P.G., 1976. Dynamic motions near an earthquake fault: a three dimensional solution. Bull. Seismol. Soc. Am. 66, 1–32.
Ruina, A.L., 1983. Slip instability and state variable friction laws. J. Geophys. Res. 88 (B12), 10,359–10,370.
Rutter, E.H., 1976. The kinetics of rock deformation by pressure solution. Phil. Trans. Roy. Soc. Lond. 283, 203–219.
Samuelson, J., Elsworth, D., Marone, C., 2009. Shear-induced dilatancy of fluid saturated faults: Experiment and theory. J. Geophys. Res. 114, B12404. doi:10.1029/2008JB006273.
Seeton, C.J., 2006. Viscosity–temperature correlation for liquids. Tribol. Lett. 22 (1). doi:10.1007/ /s11249–006–9071–2.
Segall, P., Rice, J.R., 1995. Dilatancy, compaction, and slip instability of a fluid-infiltrated fault. J. Geophys. Res. 100, 22,155–22,171.
Segall, P., Rice, J.R., 2006. Does shear heating of pore fluid contribute to earthquake nucleation? J. Geophys. Res. 111, B09316. doi:10.1029/2005JB004129.
Sibson, R.H., 2003. Thickness of the seismic slip zone. Bull. Seismol. Soc. Am. 93 (3), 1169–1178.
Sibson, R.H., Toy, V., 2006. The habitat of fault-generated pseudotachylyte presence vs. absence of friction melt. In: Abercrombie, R., McGarr, A., Di Toro, G., Kanamori, H. (Eds.), Radiated Energy and the Physics of Faulting. Geophysical Monograph Series, vol. 170. AGU, Washington, D.C., USA, pp. 153–166.
Sleep, N.H., 1995. Ductile creep, compaction, and rate and state dependent friction within major fault zones. J. Geophys. Res. 100 (B7), 13,065–13,080.
Sone, H., Shimamoto, T., 2009. Frictional resistance of faults during accelerating and decelerating earthquake slip. Nat. Geosci. doi:10.1038/NGEO637.
Sulem, J., Famin, V., 2009. Thermal decomposition of carbonates in fault zones: slip-weakening and temperature limiting effects. J. Geophys. Res. 114, B03309. doi:10.1029/2008JB006004.
Tanikawa, W., Mukoyoshi, H., Tadai, O., 2012. Experimental investigation of the influence of slip velocity and temperature on permeability, during and after high-velocity fault slip. J. Struct. Geol 38, 90–101.
Wibberley, C.A.J., Shimamoto, T., 2003. Internal structure and permeability of major strike-slip fault zones: the median tectonic line in Mie Prefecture, southwest Japan. J. Struct. Geol. 25, 59–78.
Wibberley, C.A.J., Shimamoto, T., 2005. Earthquake slip-weakening and asperities explained by thermal pressurization. Nature 436 (4), 689–792. doi:10.1038/nature03901.
Zhang, S., Tullis, T.E., Scruggs, V.J., 1999. Permeability anisotropy and pressure dependency of permeability in experimentally sheared gouge materials. J. Struct. Geol. 21, 795–806.